A modified FCCS procedure applied to Ly49A-MHC class I *cis*-interaction studies in cell membranes

Johan Strömqvist[1*], Sofia Johansson[1*], Lei Xu[1], Yu Ohsugi[2], Katja Andersson[3], Hideki Muto[2], Masataka Kinjo[2], Petter Höglund[3], Jerker Widengren[1+]

[*]*Contributed equally to this study.*
[+]*Corresponding author*
[1]*Experimental Biomolecular Physics, Department of Applied Physics, Royal Institute of Technology, AlbaNova University Center, S-10691 Stockholm, Sweden,* [2]*Laboratory of Supramolecular Biophysics, R.I.E.S, Hokkaido University, N12W6, Kita-Ku, Sapporo 060-0812, Japan,* [3]*Department of Microbiology Tumor and cell Biology (MTC), Box 280, Karolinska Institutet, S-171 77 Stockholm, Sweden*

1. Abstract

The activity of Natural Killer (NK) cells is regulated by a fine-tuned balance between activating and inhibitory receptors. Dual-colour fluorescence cross-correlation spectroscopy (FCCS) was used to directly demonstrate a so-called *cis*-interaction between a member of the inhibitory NK cell receptor family Ly49 (Ly49A), and its ligand, the Major Histocompatibility Complex (MHC) class I, within the plasma membrane of the same cell. By a refined FCCS model, calibrated by positive and negative control experiments on cells from the same lymphoid cell line, concentrations and diffusion coefficients of free and interacting proteins could be determined on a collection of cells. Using the intrinsic inter-cellular variation of their expression levels for titration, it was found that the fraction of Ly49A receptors bound in *cis* increase with increasing amounts of MHC class I ligand. This increase shows a tendency to be more abrupt than for a diffusion-limited three-dimensional bimolecular reaction, which most likely reflects the two-dimensional confinement of the reaction. For the Ly49A- MHC class I interaction it indicates that within a critical concentration range the local concentration level of MHC class I can provide a distinct regulation mechanism of the NK cell activity.

2. Introduction

Membrane proteins is a dominating group of targets for current and novel drugs and therapeutic approaches, involved in almost all cellular mechanisms. It is therefore highly relevant to characterize these proteins, with respect to their structural properties and expression levels, but also in terms of their dynamics and interaction patterns in the context of living cells. Fluorescence methods have proven to be invaluable for *in vivo* studies of protein interactions [1]. Examples are co-localization measurements based on statistical analyses of dual colour fluorescence microscopy images [2], Förster (or fluorescence) resonance energy transfer (FRET) [3, 4], and bimolecular fluorescence complementation (BiFC) assays [5]. FRET imaging is a highly specific and effective measure of short-range (<10 nm) molecular interactions. However, if the interacting proteins are large, the distance between their labels may exceed the range over which FRET occurs. BiFC is based on the association of two fragments of a fluorescent protein, to which the interacting proteins are fused. When the two proteins interact, the fragments can associate, which renders the associated protein fluorescent. The protein interaction under study may however be either facilitated or disturbed by the BiFC fragment association, which makes it difficult to estimate the absolute strength of the interaction. Both FRET and BiFC thus primarily provide qualitative information about protein interactions, but quantitative information is not easily deduced. However, quantitative information would be important, for instance to in an objective manner compare the binding strength of two different ligands binding to the same receptor, or the amount of binding of the same reactants, but under different conditions.

Fluorescence Correlation Spectroscopy (FCS) can be used to attain additional information about molecular interactions. With FCS, the mobility of single fluorescent molecules is detected by analysing the fluorescence fluctuations generated as individual molecules diffuse into and out of a typically confocal detection volume [6-9]. By dual-color Fluorescence Cross-Correlation Spectroscopy (FCCS) [10], the interaction between two molecular species, emitting in two spectrally separated bands, is analysed. Such interactions can be distinctly evidenced, not only by mere co-localization, but also by the concerted movement of the two species into and out of the detection volume, generating correlated fluorescence fluctuations. FCCS has previously been used for protein interaction studies in cells [11-14], as well as in cellular membranes [15-17] (see [18] for a review). However, like FRET and BiFC, FCCS has mainly been used as a qualitative measure of protein-ligand interactions. In particular for cellular measurements, lack of unambiguous controls and the difficulty to accurately titrate the interaction partners make it difficult to correct for cross-talk and to perform other calibrations necessary for quantitative measurements.

NK cells are part of the innate immune system and can rapidly kill cancerogenic or virally infected cells. They express an array of activating and inhibitory receptors, which together control the activation of NK cells [19, 20]. One set of inhibitory receptors are specific for MHC class I. MHC class I is an immunologically important molecule, presenting peptides of all intracellular proteins to T cells. When viral peptides are presented, the cell is killed by T cells. MHC class I is therefore often downregulated by viruses or cancerogenic cells, to avoid T cell attack. However, when NK cells interact with such MHC class I deficient cells, their inhibitory receptors are not engaged, and the target cells are killed in a so-called “missing self” reaction [21]. MHC class I specific receptors belong to the Ly49 receptor family in mice and to the Killer Immunoglobulin-Like receptor (KIR) family in humans. Ly49 and KIR receptors are structurally different, but functionally equivalent, including expression characteristics and signalling pathways [22]. Differences in combinations of expressed KIR receptors and MHC class I alleles in different individuals (presumably leading to interactions of different binding strengths) have been coupled to

susceptibility to or clearance of several diseases, including autoimmunity, cancer and viral infections [23].

Ly49 receptors and MHC class I interact in *trans* when Ly49 receptors on the NK cell interact with MHC class I on the target cell. Ly49 receptors can also interact with MHC class I on the NK cell itself, a so-called *cis* interaction [24, 25]. In contrast to *trans* binding, *cis* binding does not trigger inhibitory signalling in NK cells [25]. MHC class I molecules which engage Ly49 receptors in *cis* therefore "sequester" Ly49 receptors and prevent their binding to MHC class I in *trans* [25-27]. As a result, the extent of *cis* binding directly determines the capacity of the NK cell to sense inhibitory ligands on other cells. Given the importance of inhibitory signals for NK cell activation, it is of great interest to study the *cis* interaction between Ly49 receptors and MHC class I molecules in detail. Preferentially, this should be done within the biological context where it is taking place, i.e. in the plasma membrane of a living cell. Investigations of *cis* interactions have to date predominantly been performed by indirect measurements, for instance by blocking of antibody binding, or by biochemical techniques [25, 26, 28].

In this study, FCCS was used to directly detect, and then to further characterize and understand the *cis* interaction between the receptor Ly49A and an MHC class I allele in live cells. By applying a refined FCCS model, calibrated based on positive and negative control experiments on cells from the same cell line, quantitative values of the concentrations of free and interacting proteins of both species could be determined on a large number of cells. The intrinsic inter-cellular variation of the expression levels of the interacting proteins could then be used for titration. Since both the concentrations of the receptor and ligand, and the fraction of receptors bound to ligand, was determined quantitatively it was possible to distinguish that the fraction of Ly49A receptors bound in *cis* increases with increasing amounts of MHC class I ligand expressed on the same cell. This resembles the behaviour of a diffusion-limited three-dimensional bimolecular reaction, but shows within a critical concentration range a stronger dependence on the concentration level of the ligand. This can probably be attributed to the two-dimensional confinement of the reaction. Within this critical concentration range, the local concentration level of MHC class I may thus provide a distinct regulation mechanism of the NK cell activity.

3. MATERIALS AND METHODS

3.1 Cell lines

The murine lymphoma cell line EL-4 was used for all measurements. This cell line spontaneously expresses the MHC class I molecules H-2K^b and H-2D^b, but not H-2D^d. Due to its presumed origin as a natural killer T (NKT) lymphoma, the Ly49A receptor is spontaneously expressed in a variable way on these cells [29]. The EL4 cell line was previously transfected with a fusion protein between H-2D^d and EGFP [28] (from hereon called D^d-EGFP). Cells were grown in RPMI medium supplemented with 10% fetal calf serum, 2 mM L-glutamine, 100 U/ml penicillin, 100 μg/ml streptomycin, 100 μM non-essential amino acids, and 1 mM sodium pyruvate (Invitrogen).

3.2 Antibodies and staining procedure

Anti-H-2D^d (clone 34-2-12), anti-H-2K^b (clone AF6-88.5), and anti-Ly49A (clone JR9-318) monoclonal antibodies were purchased from BD Biosciences/Pharmingen. The JR9-318 antibody binds Ly49A regardless of whether it is free or associated with H-2D^d in *cis*, in contrast to other available Ly49A antibodies [25, 28]. All antibodies were labelled with Alexa-647 using an "Alexa 647 Monoclonal Antibody Labelling Kit" (Invitrogen), following the manufacturer's protocol. The labelled antibodies were analyzed for labelling efficiency

measuring absorbance in a Microdrop spectrophotometer (Microdrop Technologies GmbH, Germany) and by FCS, yielding equivalent results for the labelling efficiency. On average, the anti-Ly49A antibody (Ly49A-ab) was found to have ~ 4 fluorophores per antibody, the anti-K^b antibody (K^b-ab) ~ 1 and the anti-D^d antibody (D^d-ab), labelled in two different batches, ~3 and ~ 6 fluorophores per antibody, respectively. The brightness ratios (which were later on used for calculating the cross-talk parameter) were 3.8 for Ly49A and either 3.3 or 6.4 for the two D^d-ab:s, compared to the K^b-ab. For the cellular measurements, cells were stained with around 10 μg/ml antibody in phosphate buffered saline (PBS) and washed by centrifugation.

3.3 Characterization of the expression patterns of the involved molecules in the EL4 cell line.

By flow cytometry, D^d-EGFP fluorescence was detected on the majority of the EL4 cells in the culture (See Fig. S1 in the supporting material, x-axes). The the expression level however varied over a large range between the cells. The origin of this heterogeneity is unknown, but it was stable over time. The EGFP fluorescence in each cell was proportional to the fluorescence using an Al647-conjugated antibody against H-$2D^d$ (Fig. S1A), suggesting expressed D^d-EGFP-molecules were well localized to the cell surface and the majority of H-$2D^d$ molecules had a functional EGFP entity. The density of Ly49A showed a similar intra-cellular variation (Fig. S1C). The expression density of Ly49A was independent of the H-$2D^d$ expression level. Cells expressing different combinations of Ly49A and H-$2D^d$ at various densities could thus easily be found within the same cell line. This variability was taken advantage of to quantify the *cis* interaction between H-$2D^d$ and Ly49A (see section 4.4). H-$2K^b$ was expressed at a more homogeneous concentration at the cell population level (Fig. S1B). However, there was enough spread in intra-cellular H-$2K^b$ concentration to allow a range of FCCS measurements at different concentrations, matching the concentration ranges of H-$2D^d$ and Ly49A.

3.4 FCS Equipment and settings

Fluorescence microscopy and FCS measurements were performed on a Confocor 3 system (Zeiss, Jena, Germany). An Ar-Ion laser (488 nm) and a HeNe laser (633 nm) were focused through a C-Apochromat 40X, NA 1.2 objective. The fluorescence was detected by two avalanche photodiodes after passage through a dichroic mirror (HFT 488/543/633), a pinhole (edge-to-edge distance 70 μm for the FCS and 300 μm for the fluorescence microscope) in the image plane, a beam splitter (NFT 545) and an emission filter in front of each detector (BP 505-530 IR and LP655). The excitation power before the objective was within the range of 1 to 10 μW for the 488 nm-line and 0.5 to 3.5 μW for the 633 nm-line.

EL-4 cells were stained with antibodies as described above. Consecutively, 50000 cells per chamber were suspended in PBS and distributed in Lab-Tek 8-well chamber-glasses (Nunc, Thermo Scientific, Langenselbold, Germany). Data was acquired in 10 second intervals. Collection intervals containing abnormal fluorescence peaks, presumably resulting from aggregates, or within which the overall fluorescence was decaying, putatively due to membrane movements, were discarded from the overall analysis. The total included measurement times ranged from 50 to 100 s per cell. Measurements were only undertaken on viable cells where the D^d-EGFP was well localized to the cell surface membrane, as judged by visual inspection in the wide-field and confocal mode. The autofluorescence, as well as the fluorescence from both EGFP and Alexa647 in the extracellular liquid and the intracellular region was negligible (data not shown).

3.5 FCCS Theory

In FCS measurements, fluctuations in the detected fluorescence intensity, $F(t)$, are typically generated as molecules diffuse in and out of a focused laser beam. These fluctuations, $\partial F(t)$, are auto-correlated according to:

$$G(\tau) = \frac{\langle (F(t) - < F(t) >)(F(t+\tau) - < F(t) >) \rangle}{\langle F(t) \rangle^2} = \frac{\langle \partial F(t) \partial F(t+\tau) \rangle}{\langle F(t) \rangle^2}, \quad (1)$$

here brackets denote time average.

For molecules undergoing diffusion in a planar area, the detected intensity fluctuations, originating from the concentration fluctuations, $\partial c(\bar{r}, t)$, of a certain species at time *t*, is given by:

$$\partial F(t) = \kappa q \int_{R^2} W(\bar{r}) \partial c(\bar{r}, t) \partial^2 r, \quad (2)$$

Here κ denote detection efficiency, q fluorescence quantum yield of the species and $W(\bar{r}) = CEF(\bar{r}) I_{exc}(\bar{r})$ is the detected fluorescence brightness distribution, a product of the excitation intensity $I_{exc}(\bar{r})$ and the collection efficiency function CEF$(\bar{r})$.

For interaction studies between two species labelled with different fluorophores, emitting in a green (*G)* and a red (*R)* spectral range, the fluorescence fluctuations in the *G* and *R* range may be cross-correlated according to:

$$G_{GR}(\tau) = \frac{\langle (F_G(t) - < F_G(t) >)(F_R(t+\tau) - < F_R(t) >) \rangle}{\langle F_G(t) \rangle \langle F_R(t) \rangle} = \frac{\langle \partial F_G(t) \partial F_R(t+\tau) \rangle}{\langle F_G(t) \rangle \langle F_R(t) \rangle} \quad (3)$$

For the case where the individual species and their complex are confined to a two-dimensional surface (Eq. 2), and assuming that: 1) $W(\bar{r})$ has a Gaussian distribution, 2) the expectation value, $\langle F(t) \rangle$, is time-independent, 3) the brightness of the green and the red species are unaffected upon binding, 4) the time-scale of binding and dissociation of the species are much slower than their passage times through the detection area and 5) only diffusion causes the fluctuations, then the cross-correlation and the autocorrelation functions of the fluorescence in *G* and *R* have the following analytical expressions [10]:

$$\begin{cases} G_{GR}(\tau)-1=\dfrac{c_{gr}Diff_{gr}^{GR}(\tau)}{A_{GR}\left(c_g+c_{gr}\right)\left(c_r+c_{gr}\right)} \\ G_R(\tau)-1=\dfrac{c_r Diff_r^{R}(\tau)+c_{gr}Diff_{gr}^{R}(\tau)}{A_R\left(c_r+c_{gr}\right)^2} \\ G_G(\tau)-1=\dfrac{c_g Diff_g^{G}(\tau)+c_{gr}Diff_{gr}^{G}(\tau)}{A_G\left(c_g+c_{gr}\right)^2} \end{cases} \quad (4A)$$

$$\begin{cases} Diff_u^{G}(\tau)=(1+\dfrac{4D_u\tau}{\omega_G^{\,2}})^{-1} \\ Diff_u^{R}(\tau)=(1+\dfrac{4D_u\tau}{\omega_R^{\,2}})^{-1} \\ Diff_{gr}^{GR}(\tau)=(1+\dfrac{4D_{gr}\tau}{(\omega_G^{\,2}+\omega_R^{\,2})/2})^{-1} \end{cases} \quad (4B)$$

Here, c_g, c_r and c_{gr} are the concentrations of the two free species and their complex, respectively. The subscript u denotes either the green (*g*), the red (*r*) or the red-and-green (*gr*) emitting species, and D_u their corresponding diffusion coefficients. The radial distances from the maximum point of $W_G(\bar{r})$ and $W_R(\bar{r})$ to where they have dropped by a factor of e^2 is denoted ω_G and ω_R, respectively. $A_G=\left(\int W_G(\bar{r})\partial^2 r\right)^2/\int W_G(\bar{r})^2\partial^2 r$ and $A_R=\left(\int W_R(\bar{r})\partial^2 r\right)^2/\int W_R(\bar{r})^2\partial^2 r$ are the effective detection areas of the green and red laser foci, and A_{GR} is the corresponding green-red detection area ($A_{GR}=\left(\int W_G(\bar{r})W_R(\bar{r}')drdr'\right)/\int W_G(\bar{r})W_R(\bar{r})dr$) when the focal overlap is perfect.

However, in particular for FCCS measurements based on excitation from two lasers, the focal overlap is typically not perfect. Moreover, considerations such as cross-talk from the green dye into the red channel and background fluorescence need also be taken into account (see Appendix):

$$\begin{cases} G_{GR}(\tau)-1=\dfrac{\dfrac{A_G A_R}{A_{GR}}c_{gr}e^{-\frac{2r_0^2}{\omega_G^2+\omega_R^2+8D_{gr}\tau}}Diff_{gr}^{GR}(\tau)+A_G K\left(c_g Diff_g^{G}(\tau)+c_{gr}Diff_{gr}^{G}(\tau)\right)}{\left(A_G\left(c_g+c_{gr}\right)+\dfrac{bg_G}{W_{\max}^G\kappa_g^G q_g}\right)\left(A_R(c_r+c_{gr})+\dfrac{bg_R}{W_{\max}^R\kappa_r^R q_r}+A_G K(c_g+c_{gr})\right)} \\ G_R(\tau)-1=\dfrac{A_R\left(c_r Diff_r^{R}(\tau)+c_{gr}Diff_{gr}^{R}(\tau)\right)+2\dfrac{A_G A_R}{A_{GR}}Kc_{gr}e^{-\frac{2r_0^2}{\omega_G^2+\omega_R^2+8D_{gr}\tau}}Diff_{gr}^{GR}(\tau)+A_G K^2\left(c_g Diff_g^{G}(\tau)+c_{gr}Diff_{gr}^{G}(\tau)\right)}{\left(A_R(c_r+c_{gr})+\dfrac{bg_R}{W_{\max}^R\kappa_r^R q_r}+A_G K(c_g+c_{gr})\right)^2} \\ G_G(\tau)-1=\dfrac{A_G\left(c_g Diff_g^{G}(\tau)+c_{gr}Diff_{gr}^{G}(\tau)\right)}{\left(A_G(c_g+c_{gr})+\dfrac{bg_G}{W_{\max}^G\kappa_g^G q_g}\right)^2} \end{cases} \quad (4C)$$

Here, $r_0=\sqrt{x_0^2+y_0^2}$ denotes the displacement between the two lasers and $K=\dfrac{W_{\max}^G\kappa_g^R q_g}{W_{\max}^R\kappa_r^R q_r}$ denotes the crosstalk parameter, where $W_{\max}^G\kappa_g^R q_g$ and $W_{\max}^R\kappa_r^R q_r$ are the brightness of the green and red species (respectively) at the center of each foci, when detected in the red channel. Further, bg_G and bg_R are the background fluorescence in the green and the red channel, respectively, when both lasers are on.

3.6 FCS Analysis

The expressions in Eq. 4C were simultaneously fitted by a non-linear least-squares optimization routine (Origin 8, OriginLab Corporation, Northampton, MA, USA) to the three correlation curves ($G_G(\tau)$, $G_R(\tau)$ and $G_{GR}(\tau)$) recorded in each FCCS experiment. In the analysis, a three-step procedure was followed where a set of experimental parameters was first determined by negative and positive control experiments, before the actual *cis*-interaction was assessed:

1) In the negative control FCCS experiments (with no *gr* species, see Fig. 1), ω_G and ω_R were fixed to the corresponding values found in the solution measurements of that particular measurement day, and c_{gr} was fixed to zero. The rest of the parameters (c_g, c_r, D_g, D_r, D_{gr}, r_0, K) were free to vary.

2) In the positive control experiments (with *gr* but with no *r* species), K was fixed to the brightness corrected average value determined from the negative controls (see section 4.3a) and c_r was fixed to zero. The rest of the variables (c_g, c_{gr}, D_g, D_r, D_{gr}, r_0, ω_G, ω_R) were free to vary.

3) In the *cis*-interaction measurements, K was fixed to the brightness corrected average value determined from the negative controls (see section 4.3a), and the parameters r_0, ω_G and ω_R were all fixed to the average values determined from the positive controls of that particular measurement day. The rest of the variables (c_g, c_r, c_{gr}, D_g, D_r, D_{gr}) were free to vary. All measurements displayed an excitation dependent dark state of EGFP in the green auto-correlation curves ($G_G(\tau)$) with a relaxation time in the ~ 0.5 ms range, as previously observed

[30, 31]. To avoid any influence from this process, the fitting of the parameters in Eq. 4C to the experimental correlation curves was restricted to correlation times longer than 5 ms. In all fittings, bg_G and bg_R were fixed to zero, due to the negligible background fluorescence.

4. Results and Discussion

4.1 Strategy

The aim of this study was to detect and quantify the amount of interaction between the NK cell receptor Ly49A, and its ligand, the MHC class I allele H-2D^d, within the plasma membrane of a single cell (so-called *cis* interaction). By labelling the two interaction partners and using dual colour FCCS, not only the fraction of *cis*-associated Ly49A could be determined, but also the concentrations and diffusion coefficients of all three species (Ly49A, H-2D^d and their *cis*-associated complex).

Three different measuring situations were employed: a positive and a negative control, and the actual test situation (Fig. 1). In all three situations, the signal from D^d-EGFP (emitting in the green channel) was correlated with the signal of an Alexa-647 labelled antibody (emitting in the red channel). As a positive control, an antibody against H-2D^d itself was used (Fig. 1, top left panel). In this situation, nearly all antibodies detected on the cell surface were expected to be bound to D^d-EGFP, giving rise to a maximum cross-correlation signal. As a negative control, an antibody against the MHC class I allele H-2K^b (naturally expressed by the EL4 cell line) was used (Fig 1, top right panel). H-2K^b and D^d-EGFP molecules do not interact with each other on the cell surface, and should therefore give rise to a minimal cross-correlation signal. Finally, detection of the *cis* interaction between D^d-EGFP and the Ly49A receptor was achieved by correlating the signal from an antibody against Ly49A with the signal from D^d-EGFP (Fig. 1, bottom panel). Hence, we could relate our test situation to controls that were using the same pairs of fluorophores, and which were measured on the same cell population.

4.2 Detection of *cis* interaction between Ly49A and H-2D^d

Following the strategy above, FCCS measurements were performed with fluorescence fluctuations from D^d-EGFP correlated with those from Al647-ab:s directed against either H-2D^d, H-2K^b, or Ly49A. Data was collected from a number of cells for each combination, displaying different concentrations of D^d-EGFP and Al647-ab. In Fig. 2, representative auto- and cross-correlations curves for test samples and controls are shown. Each row represents a certain concentration ratio between D^d-EGFP (ligands) and the respective Al647-antibody. We chose to show equal ratio:s, rather than to fix one of the concentrations, in order to allow correct estimations of the influence of for instance cross-talk. Therefore, the absolute values are differing somewhat between the example curves. In general, the D^d-EGFP concentration varied more than the Ly49- and K^b concentration did, and D^d-EGFP is thus the largest source of variation in FCS amplitudes between the different samples.

In the top row, typical cells expressing fewer D^d-EGFP molecules than bound antibodies are shown. This situation did not exist for the positive control, since the D^d-ab:s were limited by the number of D^d-EGFP:s, and were thus always fewer than the D^d-EGFP molecules. In the Ly49A - D^d-EGFP sample (Fig. 2, right column), the cross-correlation amplitude is low at this concentration ratio, indicating a low fraction of *cis*-associated Ly49A receptors. In the middle row, measurements from cells having around 4-5 D^d-EGFP ligands per antibody are shown. A cross-correlation amplitude is observed for both the positive control and the Ly49A sample (Fig. 2, left and right column, respectively). The relative amplitude is slightly lower in the Ly49A sample, indicating that not all Ly49A are *cis*-associated. Also in the bottom row,

displaying correlation curves from cells having around 20 D^d-EGFP ligands per antibody, there is a clear cross-correlation for the positive control and the Ly49A sample. In this case there is virtually no difference between the Ly49A sample and the positive control. Hence, most Ly49A can be expected to be bound in *cis*. For the K^b-ab (the negative control), only a very limited cross-correlation was observed under these three concentration ratios (Fig. 2, middle column), indicating a very small cross-talk [14, 32, 33].

Thus, by visual inspection of the recorded auto- and cross-correlation curves it can be concluded that a specific *cis* interaction between H-$2D^d$ and Ly49A can be unambiguously detected. The extent of *cis*-interaction shows a variation with the local concentrations of the species. This variation can be further analysed in a quantitative fashion. However, to perform such analyses a more detailed characterization of the FCCS parameters is required. In particular, an influence from a displacement of the foci of the two lasers, and cross-talk between the two fluorescent detection channels, could not be excluded.

4.3 Determination of parameters relevant for the quantification of *cis* interactions

The above-mentioned cross-talk and inevitable non-perfect overlap between the two excitation laser foci are acknowledged limitations of the FCCS technique, which in general make the quantification of interactions difficult. In principle, the influence of cross-talk and focal displacement can be taken into account in the analysis, as stated in the refined FCCS model of Eq. 4C. However, to take advantage of this model, the displacement parameter r_0 and the cross-talk parameter K have to be known. Instead of adding complex techniques to determine the displacement or use approximate methods to estimate the cross-talk, we took advantage of an entirely cell-based assay to find these two parameters.

4.3a Determination of the cross-talk parameter

Cross-talk between the two fluorescent detection channels gives rise to an increased apparent cross-correlation amplitude, which could thus be interpreted as a false-positive interaction in particular when the concentration of D^d-EGFP was much higher than that of the Al647-ab. In our study the cross-talk parameter, K , is given by the ratio between the brightness of the D^d-EGFP and the Al647-labelled antibody, as detected in the red channel for both species. It could be directly determined by fitting Eq. 4C to the auto- and cross-correlation curves from the negative control, assuming that no reactions occur between the red and the green molecules (see section 3.6). With the excitation intensities used in this study, fluorescence saturation can be neglected. $W^G_{\max}\kappa^R_g q_g$ and $W^R_{\max}\kappa^R_r q_r$ and hence also K, are then proportional to the powers of the two lasers. The resulting cross-talk parameter, for a power ratio of one into the objective, was 0.5% +/- 0.7% (20 cells) for the K^b-ab. By knowing the relative brightness differences between the different antibodies (see section 3.2), K could be determined also for the positive control and the *cis* interaction measurements. The crosstalk parameters per power ratio unit were determined to 0.2% +/- 0.2% and 0.1% +/- 0.1% for the two differently labelled D^d-ab:s and 0.1% +/- 0.2% for the Ly49-ab. Thus, the cross-talk in this study was small. Apart from the fact that the emission spectra of EGFP and Al647 lies far apart from each other, a contributing reason for this is that each antibody contained several bright Al-647 fluorophores, while the D^d-EGFP only contained one EGFP.

4.3b Determination of the displacement between the focal areas

In dual laser FCCS measurements it is technically difficult to align the two lasers perfectly and a non-perfect overlap between the two detection areas is inevitable (Fig 3A). As the distance between the laser foci increases, the amplitude of the cross-correlation will decrease. In this study, the positive control provides a means to estimate the displacement between the laser foci, as all red antibodies present are expected to bind specifically to D^d-

EGFP. Hence $c_r = 0$ in Eq. 4C. By fitting Eq. 5 to the experimental auto- and cross-correlation curves in the positive control (Fig. 2, left column) with parameters set according to section 3.6, the average value of the displacement r_0 for each measurement day was determined. From these fits, also corresponding values for ω_G and ω_R could be directly determined. These average values were used in the further analysis of the *cis*-interaction between D^d-EGFP and Ly49A. The average values over all measurement days (n=35) was: 152 ± 47 nm (standard deviation) for r_0, 222 ± 51 nm for ω_G, and 270 ± 52 nm for ω_R. The most obvious reason for using the radii of the effective areas determined from the cell surface experiments, rather than the radii determined from solution measurements, is that the adjustment procedure does not necessarily place the membrane where the diameters of the laser beams are the smallest.

The determined parameter value of r_0 represents an upper limit, since also other factors could give rise to decreased cross-correlation amplitudes in the positive control measurements. In particular, if a significant fraction of the antibodies were either bound to non-fluorescing D^d-EGFP molecules, or would bind unspecifically to some other antigen on the cell surface, decreased cross-correlation amplitudes would also be observed. However, we applied a measurement strategy where the same cells and EGFP constructs were used for both controls and test samples, and provided that the unspecific binding properties of the different antibodies do not significantly differ from each other, such potential factors should have influenced both controls and test samples equally.

4.4 Quantifying the *cis* interaction between Ly49A and D^d-EGFP

Having determined the cross-talk and displacement parameters, it was possible to quantitatively determine the concentrations of Ly49A and D^d-EGFP molecules and the fraction, γ, of *cis*-associated Ly49A. In total, FCCS measurements were performed on 49 cells displaying a range of different concentrations of Ly49A and D^d-EGFP. The FCCS data was subsequently analysed as described in section 3.6. The determined parameter values are shown in Fig. 3B, with the total (bound and unbound) D^d-EGFP and Ly49A concentrations on the x- and y-axis, respectively, and the amount of *cis*-associated Ly49A indicated by the color scale. The fraction of Ly49A receptors bound in *cis* was found to vary with the concentration of D^d-EGFP, which is characteristic for a diffusion limited bimolecular reaction. For a diffusion-limited bimolecular reaction between two species A and B in solution the equilibrium constant is defined as:

$$K_D = \frac{[A_{free}] \cdot [B_{free}]}{[AB]}. \qquad (5)$$

and the fraction, γ, of bound A molecules is given by:

$$\gamma = \frac{[AB]}{[A]} = \frac{K_D + [A] + [B] + \sqrt{(K_D + [A] + [B])^2 - 4 \cdot [A] \cdot [B]}}{2[A]}. \qquad (6)$$

Here, $[A] = [A_{free}] + [AB]$ and $[B] = [B_{free}] + [AB]$ are the total concentrations of A and B, respectively, with the index *free* denoting non-bound species.
By fitting Eq. 6 to the experimentally determined parameters γ, A=Ly49A, and B=D^d-EGFP, for each of the 49 cells, K_D could be estimated to 45 ± 6 molecules/μm^2. A similar value has been determined for cytokine-receptor complexes tethered on artificial membranes [34].

In Fig. 3C, the fraction of Ly49A receptors bound in *cis* is plotted versus the D^d-EGFP concentration, regardless of the Ly49A concentration. In the cells studied, the D^d-EGFP concentration varied much more than the Ly49A concentration. As a first approximation, Fig. 3C can therefore be regarded as a binding plot for the average Ly49A concentration. With a larger span of Ly49A concentrations, the measured γ values would be expected to show a larger spread.

The red line represents the binding curve when the previously determined K_D and the average Ly49A concentration are inserted into Eq. 6. The curve reasonably resembles a bimolecular binding curve, as predicted by Eq. 6. However, the determined $K_D = 45\mu m^{-2}$ only represents an average K_D within the range of Ly49 concentrations displayed by the cells in this study. Secondly, the definition of K_D in Eq. 5 relies on that the frequency of collisions between the two reacting species is linearly dependent on the concentrations of these species. This is typically valid for reactions occurring in three dimensions, as in a solution, but is not necessarily true for a reaction confined to the two-dimensional system of a membrane [35]. Hence, Eq. 6 should be regarded as an approximate model describing the dependency of γ on [D^d-EGFP] and [Ly49A] for the *cis* interactions taking place in a cellular membrane.

Apart from variations in [Ly49A], the spread in γ can also be due to other biological variations between the cells [36-38], for instance in the metabolic state, or in the overall amount of proteins in the cell membranes (which may influence the diffusion coefficients, see below). Nonetheless, on a cell population level and according to our analysis, many cells had close to 100 % of their receptors bound in *cis* at lower D^d-EGFP concentrations than would be suggested from the fit in Fig. 3C. Presuming that the *cis* interaction is regulated by a diffusion-driven process, this probably reflects that the *cis* interaction is facilitated when the diffusion of the reactants is confined to a two-dimensional reservoir. At least within a certain concentration interval, this can render the amount of Ly49 receptors bound in *cis* even more strongly dependent on the local D^d concentration, than would be expected in solution experiments.

The error in the estimated concentrations is mainly due to the 20 % uncertainty in ω_G and ω_R (see section 4.3b). Also bleaching is expected to have some influence on the estimated concentrations. Although no significant decay in the fluorescence intensity was observed during measurements, cumulative effects could still be prominent during the measurement times [39]. Based on the low excitation power and the size of the cells (diameters of 5 to 10 μm), we estimate these cumulative effects to be less than 10%. In total, the error in the absolute concentration estimation is about 40 %. However, the error in the relative concentration estimations of the species is expected to be significantly lower.

4.5 Diffusion behaviour of MHC class I and Ly49A

Diffusion coefficients for all the involved species could be extracted from the FCCS measurements. The determined diffusion coefficients varied largely between cells, giving rise to high standard deviations. However, there was no indication that complex formation between D^d-EGFP and Ly49A would influence the diffusion rate. In the test measurements, the diffusion coefficients of "free" D^d-EGFP and Ly49A, which were not bound in a complex, were determined to 0.9 ± 0.6 $\mu m^2/s$ and 0.6 ± 0.5 $\mu m^2./s$, respectively. The diffusion coefficient of the D^d-EGFP-Ly49A complex was determined to 0.6 ± 0.3 $\mu m^2/s$. In particular for surface densities of the proteins >100 μm^{-2}, we noted that the diffusion coefficients of all three species (D^d-EGFP, Ly49A and the D^d-EGFP-Ly49A complex) decreased with higher total concentration of the species (Fig. 3D). We raised the question whether this could be due to aggregation, and if the use of bivalent antibodies by itself could give rise to formation of

antigen/antibody complexes at the cell surface, forcing molecules to diffuse as pairs rather than in isolation. However, in the positive control experiments the binding of an antibody to D^d-EGFP did not reveal any apparent difference in the diffusion coefficients between free D^d-EGFP and D^d-EGFP with an antibody bound to it (D_G compared to D_{GR} in each sample, data not shown). Moreover, a dark state relaxation process, with a characteristic time of ~0.5 ms was always present in the measured auto-correlation curves of EGFP, as previously observed in FCS measurements of GFP [30, 40]. The relative amplitude of this process was found to remain constant (~35%), and independent of the D^d-EGFP concentration. Since each fluorophore should exhibit an independent blinking behaviour, in case of oligomerization of the D^d-EGFP molecules, the amplitude of the dark state relaxation process should decrease with increased numbers of fluorophores in the complex [41, 42]. This was not observed. Taken together, no evidence was found that antibody cross-linking, or any significant aggregation of the species by other means, would be present. Instead of protein aggregation, the observed decrease in diffusion coefficients with increasing membrane protein concentrations may be related to a protein crowding effect. A decrease in the diffusion coefficients of membrane proteins, occurring above a similar membrane protein concentration range, has recently been observed in giant unilamellar vesicles [43].

5. Conclusions

We have developed practical methodologies and refined theoretical FCCS models, which allow a quantitative characterization of receptor-ligand interaction in the plasma membrane of live cells over a broad range of concentrations. By employing this strategy and exploiting the intrinsic variation in expression levels of the interacting proteins as a means for titration, we were able to quantify the specific interaction between Ly49A and D^d-EGFP in *cis* (on the membrane of the same cell). Positive and negative controls allowed us to identify the upper and lower detection limits of the system, thus enabling the identification of cells with only a small number, or virtually all, receptors bound in *cis*. Our measurements indicate a steep increase in the fraction of Ly49 receptors bound in *cis*, as the ligand concentration increase. This illustrates that the number of interactions between receptors and ligands, diffusing in a membrane, are more sensitive to variations in ligand concentrations than if the proteins would have been freely diffusing in a solution. The question of how reduced dimensionalities can influence molecular interactions is of large biological relevance. From this point of view, the strategy presented in this study may be of interest as a means to quantitatively investigate protein-protein interactions in membranes in general.

The *cis* interaction between Ly49 receptors and MHC class I is important for NK cell education, but is also interfering with the number of Ly49 receptors available to interact with MHC ligands on target cells, and thus directly affects the activation threshold of NK cells [25-27]. As a consequence, the MHC class I concentration on the NK cell itself could potentially provide a new distinct regulation mechanism of NK cell activity. At certain concentration ranges, slightly increased levels of MHC class I, for instance upon NK cell activation, could have a large influence on the fraction of *cis*-bound Ly49 receptors. Our study suggests that a two- instead of a three-dimensional reaction reservoir renders the amount of Ly49 receptors bound in *cis* even more sensitive to the local MHC class I concentration. A larger fraction of receptors bound in *cis* could in turn potentially facilitate NK cell killing. This possibility however remains to be investigated, since it is at present not known what the concentrations of Ly49 and MHC class I on native murine NK cells are, nor how they change upon NK cell activation. Nevertheless, Andersson et al previously suggested that the fraction of Ly49A receptors bound in cis on native NK cells is around 75% [28], which would place the Ly49A concentration in a range where the cis fraction would be sensitive to changes in MHC class I

concentration. Furthermore, increases in MHC class I levels have been shown to occur for instance in response to interferons, well-known NK cell activating cytokines, which are released for instance upon viral infections [44]. Whether the cis interaction is a purely diffusion driven process also in native NK cells, or rather regulated by some active biological process, is also left for future experiments to reveal.

In conclusion, our study provides an example of how refinements of ultrasensitive techniques and resulting quantitative results can lead to an increased understanding of biological mechanisms.

6. Acknowledgements

This work was supported by a Multidisciplinary BIO grant from the Foundation for Strategic Research and Vinnova (Sweden) in cooperation with Japan Science and Technology (Japan), for collaborative research, and by a grant from the Swedish Research Council (VR-NT). S. J. was supported by a postdoctoral position from the Swedish Cancer foundation. S. J. also received project funding from The Royal Swedish Academy of Sciences, Lars Hierta's foundation and Magnus Bergvall's foundation.

7. Appendix

Derivation of the dual colour cross-correlation expression for a non-perfect overlap, and when brightness differences and cross-talk are present

The detected fluorescence fluctuations, $\partial F_G(t)$ and $\partial F_R(t)$ from a set of green species and a set of red species are given by:

$$\partial F_G(t) = \sum_{u \in Set_G} k_u^G \int_{R^3} W_G(\bar{r}) \partial c_u(\bar{r},t) \partial^3 r \tag{A1}$$

$$\partial F_R(t) = \sum_{u \in Set_R} k_u^R \int_{R^3} W_R(\bar{r}-\bar{r}_0) \partial c_u(\bar{r},t) \partial^3 r + \sum_{u \in Set_G} k_u^R \int_{R^3} W_G(\bar{r}) \partial c_u(\bar{r},t) \partial^3 r \,. \tag{A2}$$

In Eq. A1 and A2 the following abbreviations have been used:
i) Set_G and Set_R are the sets of the green and red species, respectively. In case of three species, *g*, *r* and *gr*, then $Set_G = \{g, gr\}$ and $Set_R = \{r, gr\}$.
ii) $k = \kappa \cdot q$, is the product of the detection efficiency (κ) and the fluorescence quantum yield (q). More precisely: k_u^G is the probability of detecting a fluorescence photon in the green detector when a photon has been absorbed by the green fluorophore of the species *u*. k_u^R is the probability of detecting a fluorescence photon in the red detector when a photon has been absorbed by the red fluorophore of the species *u*. k_u^G is the probability of detecting a fluorescence photon in the red detector when a photon has been absorbed by the green fluorophore (due to crosstalk) of the species *u*.
iii) ∂c_u is the concentration fluctuations of species *u*.
iv) $W_G(\bar{r}) = CEF_G(\bar{r}) I_{exc,G}(\bar{r})$ and $W_R(\bar{r}) = CEF_R(\bar{r}) I_{exc,R}(\bar{r})$ are the green and the red fluorescence brightness distributions, respectively. Where $I_{exc,G}(\bar{r})$ and $I_{exc,R}(\bar{r})$ denote the excitation intensity of the laser exciting the green and the red species, respectively, and $CEF_G(\bar{r})$ and $CEF_R(\bar{r})$ signifies the collection efficiency function of the instrument in each colour range;
v) $\bar{r}_0$ is the displacement parameter, which is the distance between the centre of the green and the red laser focus.
In Eq. A2, the second summation term is due to cross-talk from the green species, detected in the red channel. The normalized $CEF_R(\bar{r}) I_{exc,G}(\bar{r})$ is assumed to be equal to the normalized $CEF_G(\bar{r}) I_{exc,G}(\bar{r})$.

Inserting Eq. A1 and Eq. A2 into the cross-correlation of the fluorescence (Eq. 3) yields:

$$G_{GR}(\tau) - 1 = \frac{\left\langle \left(\sum_{u \in Set_G} k_u^G \int_{R^3} W_G(\bar{r}) \partial c_u(\bar{r}, t+\tau) \partial^3 r \right) \left(\sum_{u \in Set_R} k_u^R \int_{R^3} W_R(\bar{r}-\bar{r}_0) \partial c_u(\bar{r},t) \partial^3 r + \sum_{u \in Set_G} k_u^R \int_{R^3} W_G(\bar{r}) \partial c_u(\bar{r},t) \partial^3 r \right) \right\rangle}{\left(\sum_{u \in Set_G} k_u^G c_u \int_{R^3} W_G(\bar{r}) \partial^3 r \right) \left(\sum_{u \in Set_R} k_u^R c_u \int_{R^3} W_R(\bar{r}) \partial^3 r + \sum_{u \in Set_G} k_u^R c_u \int_{R^3} W_G(\bar{r}) \partial^3 r \right)} \tag{A3}$$

The concentration fluctuations of two different species *u* and *v* are always uncorrelated if they are not interacting with each other, i.e. $< \partial c_u(\bar{r}', t+\tau) \partial c_v(\bar{r}, t) >= 0$ Hence:

$$G_{GR}(\tau)-1=\frac{\left(\sum_{u\in Set_G\cap Set_R}k_u^G k_u^R\int_{R^3}\int_{R^3}W_G(\bar{r})W_R(\bar{r}'-\bar{r}_0)\langle\partial c_u(\bar{r},t+\tau)\partial c_u(\bar{r}',t)\rangle\partial^3 r\partial^3 r'+\sum_{u\in Set_G}k_u^G k_u^R\int_{R^3}\int_{R^3}W_G(\bar{r})W_G(\bar{r}')\langle\partial c_u(\bar{r},t+\tau),\partial c_u(\bar{r}',t)\rangle\partial^3 r\partial^3 r'\right)}{\left(\sum_{u\in Set_G}k_u^G c_u\int_{R^3}W_G(\bar{r})\partial^3 r\right)\left(\sum_{u\in Set_R}k_u^R c_u\int_{R^3}W_R(\bar{r})\partial^3 r+\sum_{u\in Set_G}k_u^R c_u\int_{R^3}W_G(\bar{r})\partial^3 r\right)} \tag{A4}$$

Here, $Set_G\cap Set_R$, is not empty if there are double labelled species.
According to Parsevals theorem:

$$\int_{-\infty}^{\infty}f(x)g(x)^*dx=\int_{-\infty}^{\infty}F_\nu\left[f(x)\right]F_\nu\left[g(x)\right]^*d\nu, \tag{A5}$$

$F_\nu\left[f(x)\right]=\int_{-\infty}^{\infty}f(x)e^{-j\nu x}dx$ denotes the Fourier transform of $f(x)$, and star (*) indicates complex conjugation. Hence:

$$G_{GR}(\tau)-1=\frac{\left(\sum_{u\in Set_G\cap Set_R}k_u^G k_u^R\int_{R^3}\int_{R^3}W_G(\bar{r})F_\nu\left[W_R(\bar{r}'-\bar{r}_0)\right]F_\nu\left[\langle\partial c_u(\bar{r},t+\tau)\partial c_u(\bar{r}',t)\rangle\right]^*\partial^3 r\partial^3\nu+\sum_{u\in Set_G}k_u^G k_u^R\int_{R^3}\int_{R^3}W_G(\bar{r})F_\nu\left[W_G(\bar{r}')\right]F_\nu\left[\langle\partial c_u(\bar{r},t+\tau),\partial c_u(\bar{r}',t)\rangle\right]^*\partial^3 r\partial^3\nu\right)}{\left(\sum_{u\in Set_G}k_u^G c_u\int_{R^3}W_G(\bar{r})\partial^3 r\right)\left(\sum_{u\in Set_R}k_u^R c_u\int_{R^3}W_R(\bar{r})\partial^3 r+\sum_{u\in Set_G}k_u^R c_u\int_{R^3}W_G(\bar{r})\partial^3 r\right)}=$$

$$\frac{\left(\sum_{u\in Set_G\cap Set_R}k_u^G k_u^R\int_{R^3}\int_{R^3}W_G(\bar{r})e^{-j\bar{\nu}\bar{r}_0}F_\nu\left[W_R(\bar{r}')\right]c_u e^{-D_u\bar{\nu}^2\tau}e^{-j\bar{\nu}\bar{r}}\partial^3 r\partial^3\nu+\sum_{u\in Set_G}k_u^G k_u^R\int_{R^3}\int_{R^3}W_G(\bar{r})F_\nu\left[W_G(\bar{r}')\right]c_u e^{-D_u\bar{\nu}^2\tau}e^{-j\bar{\nu}\bar{r}}\partial^3 r\partial^3\nu\right)}{\left(\sum_{u\in Set_G}k_u^G c_u\int_{R^3}W_G(\bar{r})\partial^3 r\right)\left(\sum_{u\in Set_R}k_u^R c_u\int_{R^3}W_R(\bar{r})\partial^3 r+\sum_{u\in Set_G}k_u^R c_u\int_{R^3}W_G(\bar{r})\partial^3 r\right)}=$$

$$\frac{\left(\sum_{u\in Set_G\cap Set_R}k_u^G k_u^R\int_{R^3}F_\nu\left[W_G(\bar{r})\right]F_\nu\left[W_R(\bar{r}')\right]c_u e^{-D_u\bar{\nu}^2\tau-j\bar{\nu}\bar{r}_0}\partial^3\nu+\sum_{u\in Set_G}k_u^G k_u^R\int_{R^3}F_\nu\left[W_G(\bar{r})\right]F_\nu\left[W_G(\bar{r}')\right]c_u e^{-D_u\bar{\nu}^2\tau}\partial^3\nu\right)}{\left(\sum_{u\in Set_G}k_u^G c_u\int_{R^3}W_G(\bar{r})\partial^3 r\right)\left(\sum_{u\in Set_R}k_u^R c_u\int_{R^3}W_R(\bar{r})\partial^3 r+\sum_{u\in Set_G}k_u^R c_u\int_{R^3}W_G(\bar{r})\partial^3 r\right)} \tag{A6}$$

In Eq. A6, standard rules for Fourier transforms were applied, except for

$$F_\nu\left[\langle\partial c_u(\bar{r}',t)\partial c_u(\bar{r},t+\tau)\rangle\right]=c_u e^{-D_u\bar{\nu}^2\tau}e^{-j\bar{\nu}\bar{r}}. \tag{A7}$$

which is derived in reference [6].

Suppose that the excitation profile has a gaussian distribution, i.e. $W(x,y,z)=W_{\max}e^{-2\left(\frac{x^2+y^2}{\omega_{xy}^2}+\frac{z^2}{\omega_z^2}\right)}$.

Then $F_\nu\left[W(\bar{r})\right]=W_{\max}\omega^2 z_0 e^{-(\nu_x^2\omega_{xy}^2+\nu_y^2\omega_{xy}^2+\nu_z^2\omega_z^2)/8}/8$, $\int_{R^3}W(\bar{r})\partial^3 r=W_{\max}\left(\frac{\pi}{2}\right)^{3/2}\omega_{xy}^2\omega_z$ and Eq. A6 can be transformed into:

$$G_{GR}(\tau)-1=\frac{\left(\sum_{u\in Set_G\cap Set_R}k_u^G k_u^R\int_{R^3}\frac{\omega_G^2 z_G\omega_R^2 z_R c_u e^{-(\nu_x^2(\omega_G^2+\omega_R^2)/8+\nu_y^2(\omega_G^2+\omega_R^2)/8+\nu_z^2(z_G^2+z_R^2)/8+D_u\bar{\nu}^2\tau+j\bar{\nu}\bar{r}_0)}}{8^2}\partial^3\nu+\sum_{u\in Set_G}k_u^G k_u^R\left(\frac{W_{\max}^G}{W_{\max}^R}\right)^2\int_{R^3}\int_{R^3}\frac{\omega_G^4 z_G^2 c_u e^{-(\nu_x^2\omega_G^2/4+2\nu_y^2\omega_G^2/4+2\nu_z^2 z_G^2/4+D_u\bar{\nu}^2\tau)}}{8^2}\partial^3\nu\right)}{\left(\left(\frac{\pi}{2}\right)^{3/2}\omega_G^2 z_G\sum_{u\in Set_G}k_u^G c_u\right)\left(\left(\frac{\pi}{2}\right)^{3/2}\omega_R^2 z_R\sum_{u\in Set_R}k_u^R c_u+\left(\frac{\pi}{2}\right)^{3/2}\omega_G^2 z_G\frac{W_{\max}^G}{W_{\max}^R}\sum_{u\in Set_G}k_u^R c_u\right)} \tag{A8}$$

By integrating along a rectangular contour in the complex plane, the complex integral of Eq. A8 can be written:

$$\int_{-\infty}^{\infty} e^{-(\nu_x^2(\omega_G^2+\omega_R^2)/8+D_u\nu_x^2\tau+j\nu_x x_0)}\partial\nu_x = \sqrt{\frac{8\pi}{\omega_G^2+\omega_R^2}}e^{-\frac{2x_0^2}{\omega_G^2+\omega_R^2+8D_u}}\left(1+\frac{8D_u\tau}{\omega_G^2+\omega_R^2}\right)^{-1/2} \quad . \qquad \text{(A9)}$$

Inserting Eq. A9 into Eq. A8 yields the following expression for the cross correlation:

$$G_{GR}(\tau)-1=\frac{\left(\frac{V_G V_R}{V_{GR}}\sum_{u\in Set_G\cap Set_R}k_u^G k_u^R c_u e^{-\frac{2x_0^2+2y_0^2}{\omega_G^2+\omega_R^2+8D_u\tau}-\frac{2z_0^2}{z_G^2+z_R^2+8D_u\tau}}Diff_u^{GR}(\tau)\right)+\left(V_G\frac{W_{\max}^G}{W_{\max}^R}\sum_{u\in Set_G}k_u^G k_u^R c_u Diff_u^G(\tau)\right)}{\left(V_G\sum_{u\in Set_G}k_u^G c_u\right)\left(V_R\sum_{u\in Set_R}k_u^R c_u+V_G\frac{W_{\max}^G}{W_{\max}^R}\sum_{u\in Set_G}k_u^R c_u\right)}$$

.

(A10A)

$$Diff_u^G=\left(1+\frac{4D_u\tau}{\omega_G^2}\right)^{-1}\left(1+\frac{4D_u\tau}{z_G^2}\right)^{-1/2}$$

$$Diff_u^R=\left(1+\frac{4D_u\tau}{\omega_R^2}\right)^{-1}\left(1+\frac{4D_u\tau}{z_R^2}\right)^{-1/2} \qquad \text{(A10B)}$$

$$Diff_u^{GR}=\left(1+\frac{8D_u\tau}{\omega_G^2+\omega_R^2}\right)^{-1}\left(1+\frac{8D_u\tau}{z_G^2+z_R^2}\right)^{-1/2}$$

$$V_G=\pi^{3/2}\omega_G^2 z_G$$

$$V_R=\pi^{3/2}\omega_R^2 z_R \qquad \text{(A10C)}$$

$$V_{GR}=\left(\frac{\pi}{2}\right)^{3/2}(\omega_G^2+\omega_R^2)\sqrt{z_G^2+z_R^2}$$

With the same approach, the autocorrelation functions of the green and red fluorescence were obtained:

$$G_R(\tau)-1=\frac{\left(V_R\sum_{u\in Set_R}(k_u^R)^2 c_u Diff_u^R(\tau)\right)+\left(2\frac{V_G V_R}{V_{GR}}\frac{W_{\max}^G}{W_{\max}^R}\sum_{u\in Set_G\cap Set_R}k_u^R\kappa_u^G c_u Diff_u^{GR}(\tau)\,e^{-\frac{2(x_0^2+y_0^2)}{\omega_G^2+\omega_R^2+8D_u\tau}-\frac{2z_0^2}{z_G^2+z_R^2+8D_u\tau}}\right)+\left(V_G\left(\frac{W_{\max}^G}{W_{\max}^R}\right)^2\sum_{u\in Set_G}k_u^{R2}c_u Diff_u^G(\tau)\right)}{\left(V_R\sum_{u\in R}q_u^R c_u+V_G\frac{W_{\max}^G}{W_{\max}^R}\sum_{u\in G}\overset{c.t.}{\overbrace{\kappa_u^R}}q_u^G c_u\right)^2}$$

(A11)

$$G_G(\tau)-1=\frac{V_G\sum_{u\in G}(\kappa_u^G q_u^G)^2 c_u Diff_u^G(\tau)}{\left(V_G\sum_{u\in G}\kappa_u^G q_u^G c_u\right)^2} \qquad \text{(A12)}$$

The comment c.t. has been inserted into Eq. A10a and A11 to avoid ambiguities. Whenever a detection efficiency is marked with c.t., it should be clear that it is the detection efficiency of the green fluorescence detected in the red channel. Note that background intensity is implicitly included in the

general correlation expressions of Eq. A10A, A11 and A12, since background intensity can be regarded as species with infinite diffusion coefficients.

In the case of two-dimensional diffusion, the effective volumes (V_G , V_R and V_{GR}) should be replaced with the effective areas (A_G , A_R and A_{GR}) in Eq. A10A, A11 and A12, and z_G and z_R should be replaced with infinity in Eq. A10A, A10B, A11, and A12.

References

1. Hebert, T.E., C. Gales, and R.V. Rebois, *Detecting and imaging protein-protein interactions during g protein-mediated signal transduction in vivo and in situ by using fluorescence-based techniques.* Cell Biochemistry and Biophysics, 2006. **45**(1): p. 85-109.
2. Comeau, J.W.D., S. Costantino, and P.W. Wiseman, *A guide to accurate fluorescence microscopy colocalization measurements.* Biophysical Journal, 2006. **91**(12): p. 4611-4622.
3. Periasamy, A., H. Wallrabe, Y. Chen, and M. Barroso, *Quantitation of Protein-Protein Interactions: Confocal FRET Microscopy*, in *Biophysical Tools for Biologists, Vol 2: In Vivo Techniques*. 2008, ELSEVIER ACADEMIC PRESS INC: San Diego. p. 569-+.
4. Vamosi, G., A. Bodnar, G. Vereb, A. Jenei, C.K. Goldman, J. Langowski, K. Toth, L. Matyus, J. Szollosi, T.A. Waldmann, and S. Damjanovich, *IL-2 and IL-15 receptor alpha-subunits are coexpressed in a supramolecular receptor cluster in lipid rafts of T cells.* Proceedings of the National Academy of Sciences of the United States of America, 2004. **101**(30): p. 11082-11087.
5. Kerppola, T.K., *Bimolecular fluorescence complementatlon: Visualization of molecular interactions in living cells*, in *Fluorescent Proteins, Second Edition*. 2008, ELSEVIER ACADEMIC PRESS INC: San Diego. p. 431-+.
6. Magde, D., E.L. Elson, and W.W. Webb, *Thermodynamic fluctuations in a reacting system - measurement by fluorescence correlation spectroscopy.* Physical Review Letters, 1972. **29**: p. 705-711.
7. Rigler, R., U. Mets, J. Widengren, and P. Kask, *Fluorescence Correlation Spectroscopy with High Count Rate and Low-Background - Analysis of Translational Diffusion.* European Biophysics Journal with Biophysics Letters, 1993. **22**(3): p. 169-175.
8. Haustein, E. and P. Schwille, *Fluorescence correlation spectroscopy: Novel variations of an established technique.* Annual Review of Biophysics and Biomolecular Structure, 2007. **36**: p. 151-169.
9. Chen, H.M., E.R. Farkas, and W.W. Webb, *In Vivo Applications of Fluorescence Correlation Spectroscopy*, in *Biophysical Tools for Biologists, Vol 2: In Vivo Techniques*. 2008, ELSEVIER ACADEMIC PRESS INC: San Diego. p. 3-+.
10. Schwille, P., F.J. MeyerAlmes, and R. Rigler, *Dual-color fluorescence cross-correlation spectroscopy for multicomponent diffusional analysis in solution.* Biophysical Journal, 1997. **72**(4): p. 1878-1886.
11. Kim, S.A., K.G. Heinze, M.N. Waxham, and P. Schwille, *Intracellular calmodulin availability accessed with two-photon cross-correlation.* Proceedings of the National Academy of Sciences of the United States of America, 2004. **101**(1): p. 105-110.
12. Kim, S.A., K.G. Heinze, K. Bacia, M.N. Waxham, and P. Schwille, *Two-photon cross-correlation analysis of intracellular reactions with variable stoichiometry.* Biophysical Journal, 2005. **88**(6): p. 4319-4336.
13. Saito, K., I. Wada, M. Tamura, and M. Kinjo, *Direct detection of caspase-3 activation in single live cells by cross-correlation analysis.* Biochemical and Biophysical Research Communications, 2004. **324**(2): p. 849-854.
14. Baudendistel, N., G. Muller, W. Waldeck, P. Angel, and J. Langowski, *Two-hybrid fluorescence cross-correlation spectroscopy detects protein-protein interactions in vivo.* Chemphyschem, 2005. **6**(5): p. 984-990.

15. Vukojevic, V., Y. Ming, C. D'Addario, M. Hansen, U. Langel, R. Schulz, B. Johansson, R. Rigler, and L. Terenius, *mu-opioid receptor activation in live cells.* Faseb Journal, 2008. **22**(10): p. 3537-3548.
16. Neugart, F., A. Zappe, D.M. Buk, I. Ziegler, S. Steinert, M. Schumacher, E. Schopf, R. Bessey, K. Wurster, C. Tietz, M. Borsch, J. Wrachtrup, and L. Graeve, *Detection of ligand-induced CNTF receptor dimers in living cells by fluorescence cross correlation spectroscopy.* Biochimica Et Biophysica Acta-Biomembranes, 2009. **1788**(9): p. 1890-1900.
17. Liu, P., T. Sudhaharan, R.M.L. Koh, L.C. Hwang, S. Ahmed, I.N. Maruyama, and T. Wohland, *Investigation of the dimerization of proteins from the epidermal growth factor receptor family by single wavelength fluorescence cross-correlation spectroscopy.* Biophysical Journal, 2007. **93**(2): p. 684-698.
18. Hwang, L.C. and T. Wohland, *Recent advances in fluorescence cross-correlation spectroscopy.* Cell Biochemistry and Biophysics, 2007. **49**(1): p. 1-13.
19. Bryceson, Y.T. and E.O. Long, *Line of attack: NK cell specificity and integration of signals.* Curr Opin Immunol, 2008. **20**(3): p. 344-52.
20. Lanier, L.L., *Up on the tightrope: natural killer cell activation and inhibition.* Nat Immunol, 2008. **9**(5): p. 495-502.
21. Kärre, K., H.G. Ljunggren, G. Piontek, and R. Kiessling, *Selective rejection of H-2-deficient lymphoma variants suggests alternative immune defence strategy.* Nature, 1986. **319**(6055): p. 675-8.
22. Joncker, N.T. and D.H. Raulet, *Regulation of NK cell responsiveness to achieve self-tolerance and maximal responses to diseased target cells.* Immunol Rev, 2008. **224**: p. 85-97.
23. Boyton, R.J. and D.M. Altmann, *Natural killer cells, killer immunoglobulin-like receptors and human leucocyte antigen class I in disease.* Clin Exp Immunol, 2007. **149**(1): p. 1-8.
24. Zimmer, J., V. Ioannidis, and W. Held, *H-2D ligand expression by Ly49A+ natural killer (NK) cells precludes ligand uptake from environmental cells: implications for NK cell function.* J Exp Med, 2001. **194**(10): p. 1531-9.
25. Doucey, M.A., L. Scarpellino, J. Zimmer, P. Guillaume, I.F. Luescher, C. Bron, and W. Held, *Cis association of Ly49A with MHC class I restricts natural killer cell inhibition.* Nat Immunol, 2004. **5**(3): p. 328-36.
26. Chalifour, A., L. Scarpellino, J. Back, P. Brodin, E. Devevre, F. Gros, F. Levy, G. Leclercq, P. Hoglund, F. Beermann, and W. Held, *A Role for cis Interaction between the Inhibitory Ly49A Receptor and MHC Class I for Natural Killer Cell Education.* Immunity, 2009.
27. Back, J., A. Chalifour, L. Scarpellino, and W. Held, *Stable masking by H-2Dd cis ligand limits Ly49A relocalization to the site of NK cell/target cell contact.* Proc Natl Acad Sci U S A, 2007. **104**(10): p. 3978-83.
28. Andersson, K.E., G.S. Williams, D.M. Davis, and P. Hoglund, *Quantifying the reduction in accessibility of the inhibitory NK cell receptor Ly49A caused by binding MHC class I proteins in cis.* Eur J Immunol, 2007. **37**(2): p. 516-27.
29. Gays, F., M. Unnikrishnan, S. Shrestha, K.P. Fraser, A.R. Brown, C.M.G. Tristram, Z.M.A. Chrzanoveska-Lightowlers, and C.G. Brooks, *The mouse tumor cell lines EL4 and RMA display mosaic expression of NK-related and certain other surface molecules and appear to have a common origin.* Journal of Immunology, 2000. **164**(10): p. 5094-5102.
30. Haupts, U., S. Maiti, P. Schwille, and W.W. Webb, *Dynamics of fluorescence fluctuations in green fluorescent protein observed by fluorescence correlation*

spectroscopy. Proceedings of the National Academy of Sciences of the United States of America, 1998. **95**(23): p. 13573-13578.
31. Widengren, J., B. Terry, and R. Rigler, *Protonation kinetics of GFP and FITC investigated by FCS - aspects of the use of fluorescent indicators for measuring pH.* Chemical Physics, 1999. **249**(2-3): p. 259-271.
32. Bacia, K. and P. Schwille, *A dynamic view of cellular processes by in vivo fluorescence auto- and cross-correlation spectroscopy.* Methods, 2003. **29**(1): p. 74-85.
33. Weidemann, T., M. Wachsmuth, M. Tewes, K. Rippe, and J. Langowski, *Analysis of ligand binding by two-colour fluorescence cross-correlation spectroscopy.* Single Molecules, 2002. **3**(1): p. 49-61.
34. Gavutis, M., S. Lata, E. Jaks, P. Lamken, and J. Piehler, *Dynamics of cytokine-receptor complexes on model membranes.* Biophysical Journal, 2005. **88**(1): p. 532A-532A.
35. Naqvi, K.R., J.-P. Behr, and D. Chapman, *Methods for probing lateral diffusion of membrane components: triplet--triplet annihilation and triplet--triplet energy transfer.* Chemical Physics Letters, 1974. **26**(3): p. 440-444.
36. Tuvia, S., A. Almagor, A. Bitler, S. Levin, R. Korenstein, and S. Yedgar, *Cell membrane fluctuations are regulated by medium macroviscosity: Evidence for a metabolic driving force.* Proceedings of the National Academy of Sciences of the United States of America, 1997. **94**(10): p. 5045-5049.
37. Krol, A.Y., M.G. Grinfeldt, S.V. Levin, and A.D. Smilgavichus, *Local Mechanical Oscillations of the Cell-Surface within the Range 0.2-30 Hz.* European Biophysics Journal, 1990. **19**(2): p. 93-99.
38. Milon, S., R. Hovius, H. Vogel, and T. Wohland, *Factors influencing fluorescence correlation spectroscopy measurements on membranes: simulations and experiments.* Chemical Physics, 2003. **288**(2-3): p. 171-186.
39. Widengren, J. and P. Thyberg, *FCS cell surface measurements - "Photophysical limitations and consequences on molecular ensembles with heterogenic mobilities.* Cytometry Part A, 2005. **68A**(2): p. 101-112.
40. Widengren, J., Ü. Mets, and R. Rigler, *Photodynamic properties of green fluorescent proteins investigated by fluorescence correlation spectroscopy.* Chemical Physics, 1999. **250**(2): p. 171-186.
41. Widengren, J., Ü. Mets, and R. Rigler, *Fluorescence Correlation Spectroscopy of Triplet-States in Solution - a Theoretical and Experimental-Study.* Journal of Physical Chemistry, 1995. **99**(36): p. 13368-13379.
42. Shimizu, M., S. Sasaki, and M. Kinjo, *Triplet fraction buildup effect of the DNA-YOYO complex studied with fluorescence correlation spectroscopy.* Analytical Biochemistry, 2007. **366**(1): p. 87-92.
43. Ramadurai, S., A. Holt, V. Krasnikov, G. van den Bogaart, J.A. Killian, and B. Poolman, *Lateral Diffusion of Membrane Proteins.* Journal of the American Chemical Society, 2009. **131**(35): p. 12650-12656.
44. Vegh, Z., P. Wang, F. Vanky, and E. Klein, *Increased expression of MHC class I molecules on human cells after short time IFN-gamma treatment.* Mol Immunol, 1993. **30**(9): p. 849-54.

FIGURE LEGENDS

Fig 1: Depiction of the molecular interactions measured: positive control (top left), negative control (top right), and the test sample (bottom). All measurements were performed on EL-4

cells, previously transfected with D^d-EGFP. Only the Alexa647-coupled antibodies varied between the different measurement scenarios. In the positive control, the signal from D^d-EGFP was detected in combination with an antibody against the very same H-$2D^d$ molecule. As a negative control, the signal from D^d-EGFP was combined with detection of an antibody against H-$2K^b$, which does not interact with H-$2D^d$. For the detection and quantification of *cis*-interaction, the signal from D^d-EGFP was combined with an antibody against Ly49A (bottom).

Fig 2: Typical auto- and cross-correlation curves of D^d-EGFP with: D^d-ab (left column), K^b-ab (middle column), and Ly49A-ab (right column). Green squares represent auto-correlation curves from D^d-EGFPs in all plots. Red circles show autocorrelation curves from Al647-labelled antibodies against: H-$2D^d$ (left), H-$2K^b$ (middle), and Ly49A (left). Orange triangles represent the corresponding cross-correlation curves between D^d-EGFP and these three species. Black lines represent the corresponding fits, according to Eq. 4C. Each column contains three different concentration ratios of receptors per ligand (except for the positive control, which only contains two different ratios), from top to bottom: 0.3 and 0.07 (left); 1.3, 0.3 and 0.05 (middle); and 1.8, 0.2 and 0.05 (right).

Fig 3: (A) Schematic figure of the two laser foci; both positioned on the cell membrane. The two excitation foci do not overlap perfectly. The distance between the centers of the foci is referred to as the displacement, r_0. The focal radii of the green and red excitation lasers (ω_G and ω_R), and r_0, was determined during the cell surface measurements (see section 4.3b). (B) Degree of *cis*-interaction between Ly49A and D^d-EGFP in relation to their concentrations in the cellular membrane. For each cell, the number of D^d-EGFP and Ly49A molecules per μm^2, and the fraction of receptors that were bound in *cis*, was determined. The x-axis shows the total D^d-EGFP concentration (both bound and unbound) and the y-axis shows the total Ly49A concentration. The fraction of receptors bound to D^d-EGFP is depicted by the color scale indicated in the legend. (C) The same data set, but now with the D^d-EGFP concentration on the x-axis and the fraction of Ly49 receptors bound in *cis* on the y-axis. The red curve is the best fit of the experimentally determined fractions γ to Eq. 7. The error bars of the concentrations are due to the uncertainty in the displacement parameter, $r_{0,}$ and denote values presuming the r_0 +/- standard deviation for the specific day. (D) Dependence of the diffusion coefficients of D^d-EGFP (green squares), Ly49A-Al647 (red circles) and their complex (orange triangles) on the concentration of total amount of Ly49A-Al647 and D^d-EGFP on the cell..

Figures:

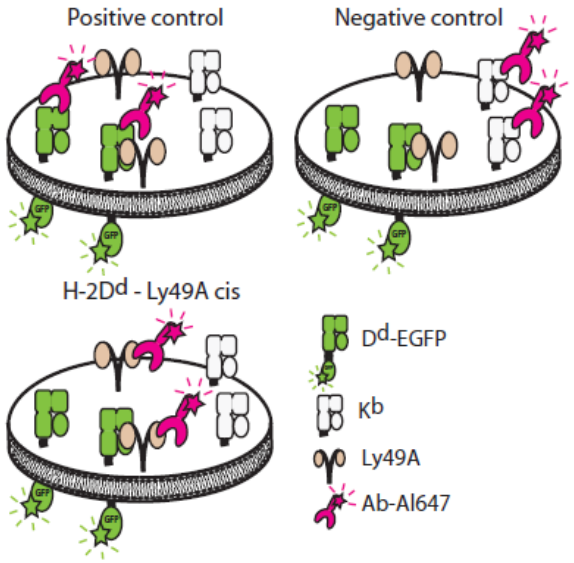

Figure 1

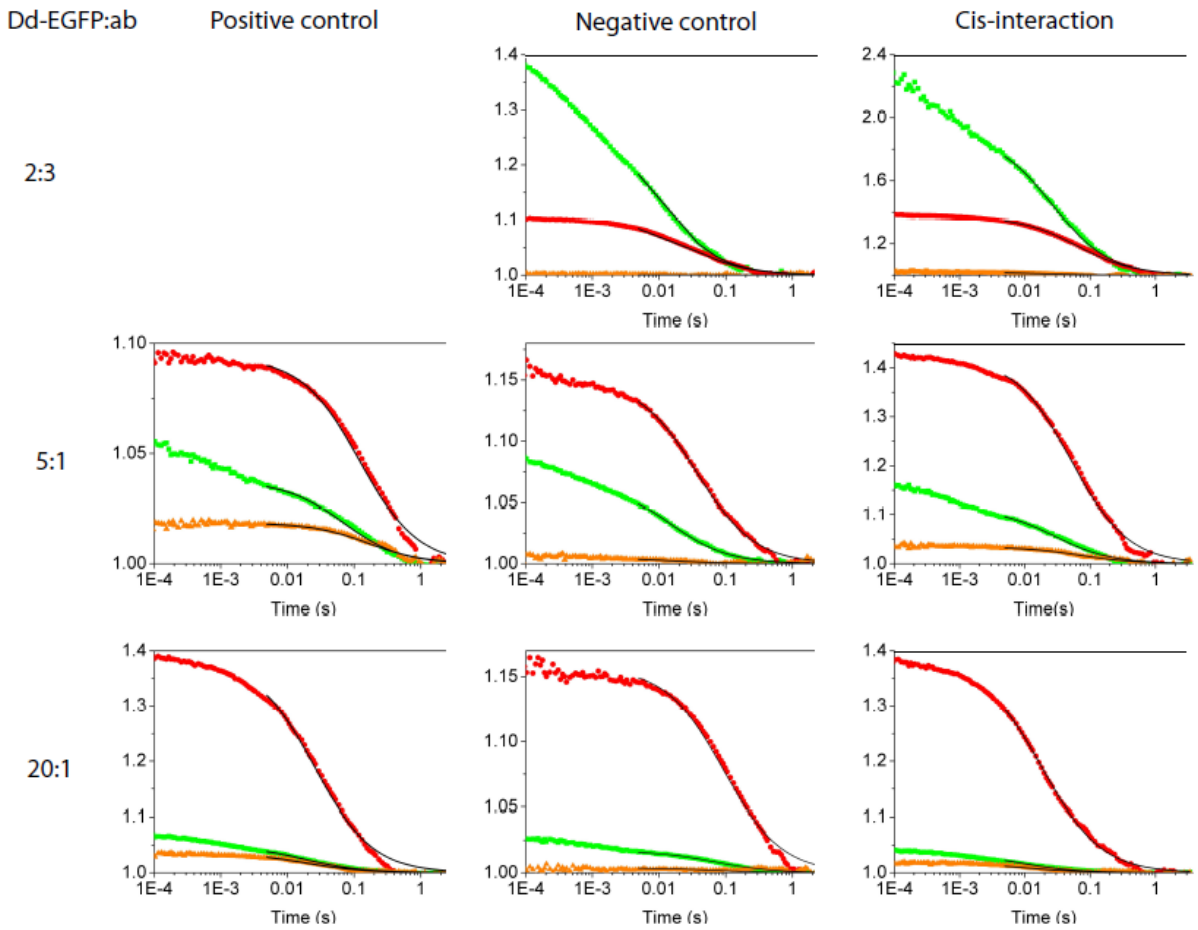

Figure 2

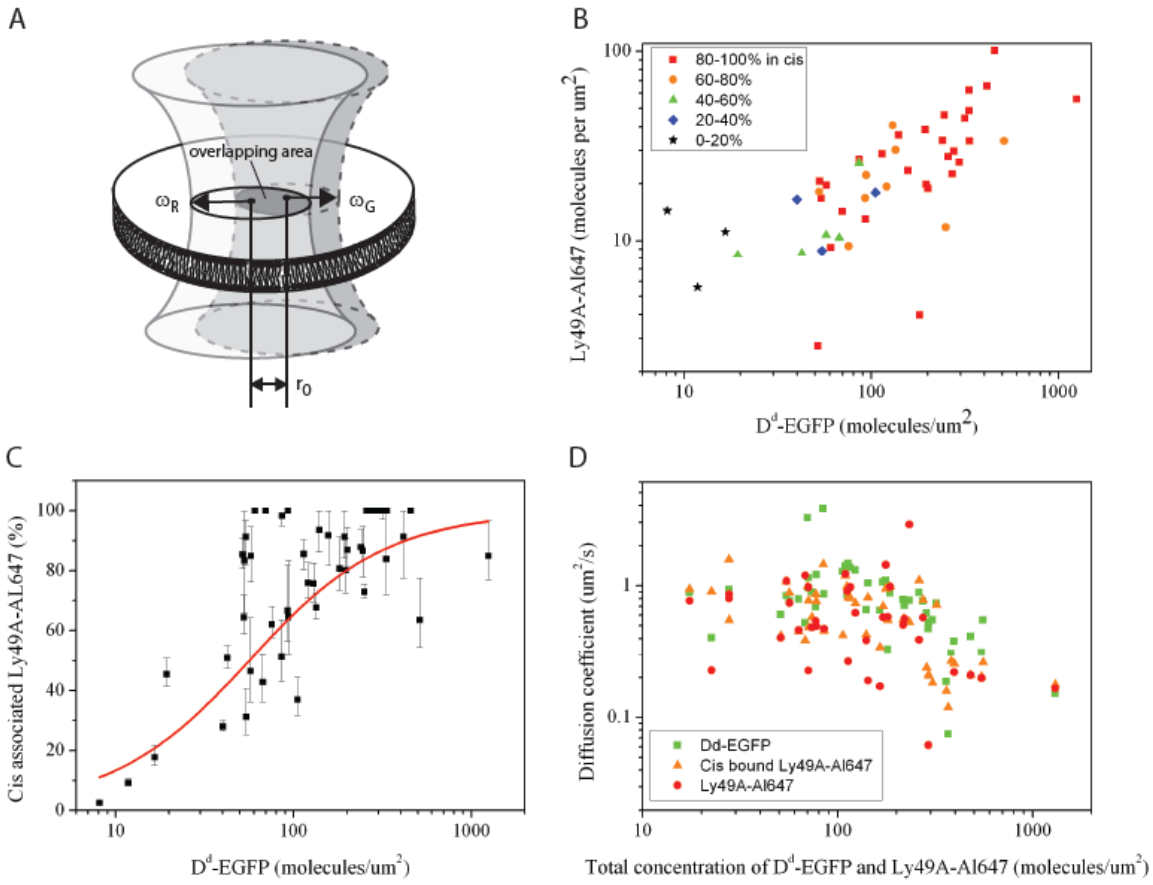
A
overlapping area
ω_R
ω_G
r_0
B
80-100% in cis
60-80%
40-60%
20-40%
0-20%
Ly49A-Al647 (molecules per um^2)
D^d-EGFP (molecules/um^2)
C
Cis associated Ly49A-AL647 (%)
D^d-EGFP (molecules/um^2)
D
Diffusion coefficient (um^2/s)
Dd-EGFP
Cis bound Ly49A-Al647
Ly49A-Al647
Total concentration of D^d-EGFP and Ly49A-Al647 (molecules/um^2)

Figure 3